Neutral Point Overvoltages in Wye-Wye Connected Distribution Transformer Caused by Lightning Current in Low-Voltage Winding

Bjørn Gustavsen, *Fellow*, Kårstein Longva

***Abstract*—Lightning strokes is a main source of transformer failures in distribution systems. The discharge of a lightning current through a distribution transformer's high-voltage (HV) side arresters leads to a ground potential rise of the transformer tank. In the case of a wye-wye connected transformer with ungrounded HV neutral point, the ground potential rise can drive a current through the low-voltage (LV) side windings that leads to an excessive voltage in the HV side neutral point by inductive transformation. Simulations by a measurement-based model demonstrate that a voltage several times the lightning impulse test voltage can arise in the neutral point, in the case of a close lightning strike to the HV side overhead line. The use of transformer LV side surge arresters in combination with proper grounding on the HV-side are effective ways of reducing the neutral point overvoltage.**

***Index Terms*—Distribution transformer, lightning stroke, ground potential rise, transformer neutral point, overvoltage.**

I. Introduction

LIGHTNING overvoltages are one of the main causes of distribution transformer failures. Although a very good understanding exists regarding the generation of overvoltages from lightning stroke currents and associated EM fields [1],[2],[3], the number of failures remains high in many locations. The failures are in part due to the limited expenditure a utility can provide in terms of protective devices and improvement of grounding structures. For instance, in some areas in Southern Norway, as much as 1% of the transformer population has failed in a single year, despite the lightning ground flash density being quite low in comparison with central European countries.

A lightning stroke to an overhead line (OHL) causes a current of several kiloamps to be injected into the line, leading to high-frequency overvoltages that will stress the insulation of a connected transformer [4],[5],[6]. Such overvoltages can emerge from either the high-voltage (HV) or low-voltage (LV) side of the transformer. In addition, nearby lightning strokes lead to induced overvoltages on the OHL by the surrounding electrical and magnetic fields [7],[8],[9]. The actual overvoltage that will appear on the transformer terminals is strongly affected by possible insulator string flashovers, the presence of cable sections, and the use of protective devices such as surge arresters.

The occurrence of a lightning overvoltage can cause transformer failure by several mechanisms [10].

1. The overvoltage is so high in peak value that the phase-to-earth insulation is unable to withstand the voltage.
2. The overvoltage is very steep-fronted, leading to excessive differential stresses near the winding entrance.
3. An oscillating component in the overvoltage causes large internal voltages by resonance.

In addition to these failure modes, there is also the possibility that the lightning stroke causes a failure via the transformer ground potential rise. One possible scenario is that the ground potential rise causes a current to flow through the LV windings, which in turn leads to a transformed voltage along the HV windings. In the case of a wye-wye connected transformer where the HV-side neutral point (N) is ungrounded, the N-point voltage can then become very high, potentially leading to insulation failure. Such situation frequently arises in Norwegian rural areas where wye-wye connected transformers are used for feeding IT-type LV systems.

The purpose of this paper is to develop a transformer model suitable for simulation of N-point overvoltages, and to demonstrate the application of the model with usage of alternative overvoltage protection methods. Fairly simple models of the surrounding network are used to make it easier to interpret the results. The considered transformer is a three-phase YNyn connected 11 kV/230 V unit. A suitable wide-band measurement-based transformer model is first presented that permits to simulate the neutral point voltage build-up vs. tank. The model is utilized within an EMTP-type simulation environment where the transformer is fed from an 11 kV overhead line (OHL) that feeds a 230 LV IT system. The N-

Manuscript received… This work was supported by the consortium participants of the SINTEF-led project "ProTrafo" (project no. 269303/E20).

B. Gustavsen is with SINTEF Energy Research, N-7465 Trondheim, Norway (e-mail: bjorn.gustavsen@sintef.no).

K. Longva is with Møre Trafo, N-6230 Sykkylven. Norway (e-mail: kaarstein.longva@moretrafo.no)

point overvoltage due to a close lightning stroke to the HV OHL is calculated. Means of reducing the overvoltage are compared, including the use of LV-side surge arresters, additional spark gaps on HV-side, and the use of a ground wire on the HV side.

II. Neutral Point Overvoltage

The neutral point overvoltage phenomenon is relevant for wye-wye connected transformers where the transformer HV-side neutral point is ungrounded. Such configurations are frequently found those countries (e.g. Norway) where the power system on both the HV-side and LV side of the distribution transformer are operated with high-impedance grounding. In such system, the neutral point overvoltage can be explained by Fig. 1. A lightning strike to the HV-side OHL close to the transformer causes the transformer HV-side surge arresters to operate. A part of the lightning current will flow to remote ground via the tank grounding impedance, causing a potential rise of the tank vs. remote ground. As a result, the LV-side n-point arrester starts conducting current which causes a current to flow through the LV windings. The associated LV winding voltage drop is transformed to the HV windings according to the transformer's voltage ratio, giving rise to a voltage in the (ungrounded) N-point since the voltages on the HV winding external terminals are effectively clamped. There will also be capacitively coupled currents, but they are not essential for the voltage transformation which is associated with the long-duration part of the lightning current. The presence of LV-side arresters (grey color in Fig. 1) will affect the current flow in the LV windings. Their impact is studied in later sections.

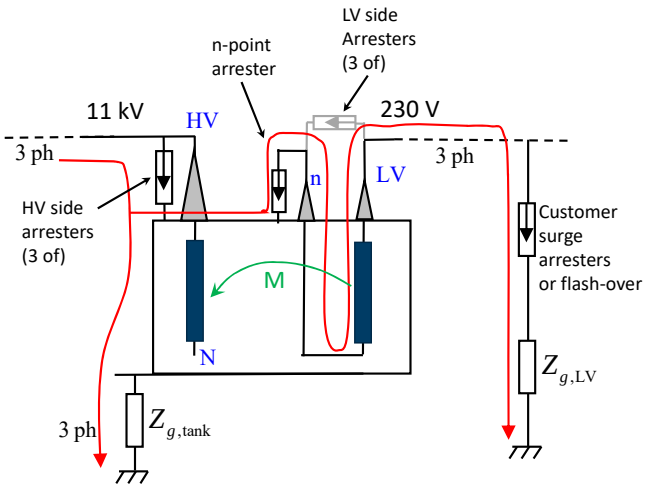

Fig. 1. Direct stroke to HV side overhead line. Considered lightning current paths and inductive voltage transformation from LV windings to HV windings.

III. Distribution Transformer

To study the N-point overvoltage phenomenon, a measurement-based model is derived of a distribution transformer. The transformer has a three-legged core, three phases, HV layer windings and LV foil windings. The LV windings are split into two sections that are wound in opposite directions. All HV and LV winding ends are brought out to external bushings, permitting reconnection into alternative vector groups. The HV winding midpoints are also brought out, allowing to measure the internal voltage at these points. The transformer and its winding layout are shown in Figs. 2 and 3, respectively. This 300 kVA transformer is in the current work connected into YNyn, giving a 11000:230 nominal voltage ratio. The lightning impulse test voltage is 75 kV (IEC 60076-3).

Fig. 4 shows a simplified schematic of the transformer layout in Fig. 3, with labeling defined by Table I. A model is to be derived that has eight external terminals (red color) for connecting to an external circuit, and four internal observation points for voltage (blue color), including the HV-side N-point.

Fig. 2. Distribution transformer. Left: HV terminals; right: LV terminals.

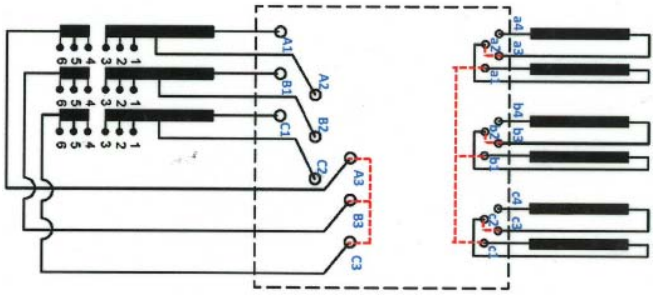

Fig. 3. Winding layout of transformer connected in YNyn.

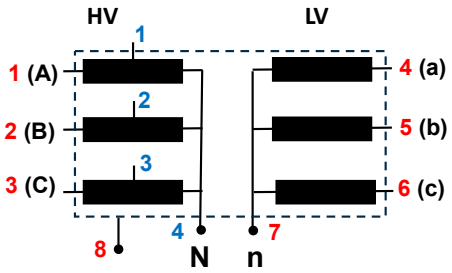

Fig. 4. Terminal numbering.

TABLE I
TERMINALS AND VOLTAGE OBSERVATION POINTS.

Terminals		Observation Points	
1	HV, phase A	1	HV midpoint, phase A
2	HV, phase B	2	HV midpoint, phase B
3	HV, phase C	3	HV midpoint, phase C
4	LV, phase A	4	HV neutral (N)
5	LV, phase B		
6	LV, phase C		
7	LV neutral (n)		
8	Tank		

IV. ADMITTANCE AND VOLTAGE TRANSFER

The reason for separating the terminals into external terminals and voltage observation nodes is that the modeling of the transformer is simplified very much. The external terminals are associated with an admittance model which must obey passivity, i.e. it must not generate power. The passivity requirement is generally easier to satisfy when the number of (external) terminals is kept low.

Voltages (node-ground) and currents at the external terminals are related via the 8×8 admittance matrix **Y** (1), while a voltage transfer block is used for relating the eight external voltages to the four internal voltages via a 4×8 transfer matrix **H** (2). The terminal equivalent is included in the time domain simulation whereas the voltage transfer block is used for calculating the voltage on additional observation points with the voltage on the external terminals taken as known quantities. Fig. 5 shows the electrical quantities associated with **Y** and **H**, with labeling as previously defined in Fig. 4 and Table 1.

$$\mathbf{i}_{\text{ext},(8\times1)}(\omega) = \mathbf{Y}_{(8\times8)}(\omega)\mathbf{v}_{\text{ext},(8\times1)}(\omega) \tag{1}$$

$$\mathbf{v}_{\text{int},(4\times1)}(\omega) = \mathbf{H}_{(4\times8)}(\omega)\mathbf{v}_{\text{ext},(8\times1)}(\omega) \tag{2}$$

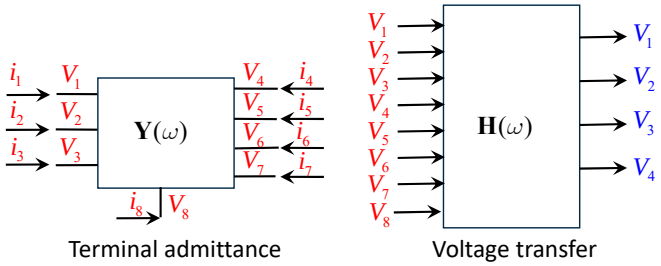

Fig. 5. Admittance model (left) and voltage transfer model (right).

V. TRANSFORMER MODELING

A wide-band model of the transformer is developed by fitting a rational model to frequency domain measurements of matrices **Y** and **H**. The measurements and fitting process consider only seven external terminals with the tank taken as ground reference. The eighth terminal (tank) is introduced afterwards by mathematical manipulation (Section V.D).

A. Measurement Setup

Frequency sweep measurements of **Y** and **H** are performed at low voltage, using a vector network analyzer, a wide-band current transformer, and voltage probes. Details of the measurement setup and procedure are outlined in the Appendix.

B. Admittance Measurements And Modeling

Fig. 6 shows by solid blue traces the 49 measured elements of the 7×7 frequency-dependent admittance matrix $\mathbf{Y}(\omega)$. Fig. 6 further shows the behavior of a pole-residue model approximation (3), denoted by dashed red traces. The model is obtained by subjecting the admittance matrix to a passivity preserving mode-revealing transformation (MRT) [11], and the resulting matrix elements were fitted with a 70th order common-pole model using vector fitting (VF) [12],[13] followed by passivity enforcement [14]. The model is afterwards subjected to MRT back-transformation to obtain the final result. The overall agreement between the data and the rational approximation is seen to be very good. A similar good agreement is also achieved for the admittance matrix eigenvalues (Fig. 7), indicating that the model can be applied with alternative terminal conditions with little chance of error magnifications.

$$\mathbf{Y}(\omega) \cong \mathbf{R}_0^Y + \sum_{n=1}^{N^Y} \frac{\mathbf{R}_n^Y}{j\omega - a_n^Y} \tag{3}$$

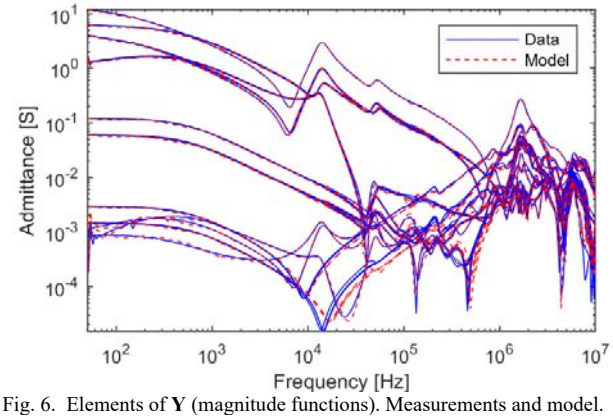

Fig. 6. Elements of **Y** (magnitude functions). Measurements and model.

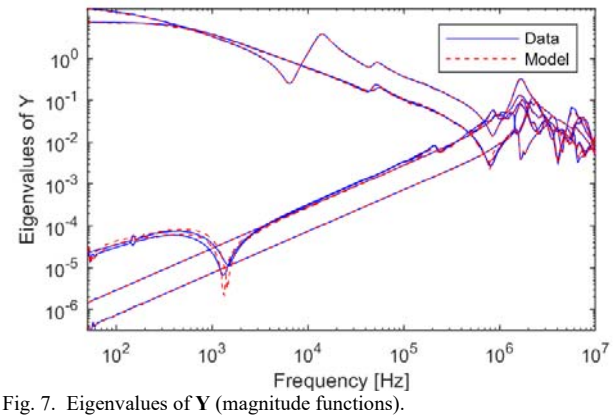

Fig. 7. Eigenvalues of **Y** (magnitude functions).

C. Voltage Transfer Measurements And Modeling

Fig. 8 shows with solid blue traces the 28 measured voltage transfer functions of the 4×7 frequency-dependent matrix $\mathbf{H}(\omega)$. The elements are fitted with a 60th order common-pole model (4). The traces of the rational approximation (dashed red) are seen to nearly superimpose the measured traces, indicating a

high-quality model extraction.

$$\mathbf{H}(\omega) \cong \mathbf{R}_0^H + \sum_{n=1}^{N^H} \frac{\mathbf{R}_n^H}{j\omega - a_n^H} \tag{4}$$

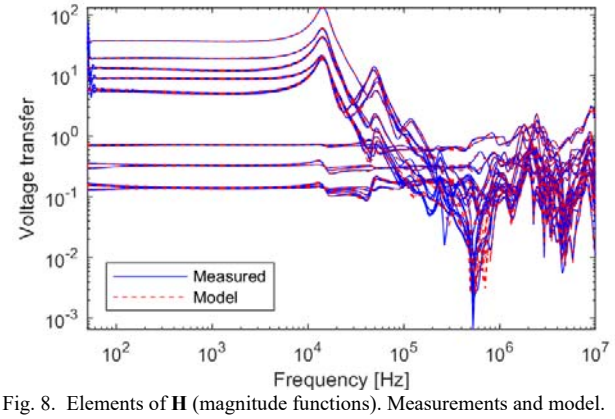

Fig. 8. Elements of **H** (magnitude functions). Measurements and model.

D. Introduction of Ground Reference Terminal

During the measurements and modeling, the transformer tank is the ground reference to which all voltages refer to. In order to simulate the effect of a ground potential rise, it is necessary to introduce an additional, eighth terminal to which a ground electrode impedance can be connected. This is achieved by augmenting the two existing models representing **H** and **Y**.

1) Voltage Transfer Model

With the tank being the voltage reference in the measurements and denoted "*r*", we can write for the voltage transfer,

$$(\mathbf{v}_{\text{int}} - \mathbf{e}_2 \cdot v_{\text{r}}) = \mathbf{H} \cdot (\mathbf{v}_{\text{ext}} - \mathbf{e}_1 \cdot v_{\text{r}}) \tag{5}$$

where $\mathbf{e}_1$ and $\mathbf{e}_2$ are vectors of ones. Solving (5) gives

$$\mathbf{v}_{\text{int}} = \mathbf{e}_2 v_{\text{r}} + \mathbf{H} \cdot (\mathbf{v}_{\text{ext}} - \mathbf{e}_1 v_{\text{r}}) \tag{6}$$

Rearranging (6) into a matrix-vector product gives

$$\mathbf{v}_{\text{int}} = \begin{bmatrix} \mathbf{H} & (\mathbf{e}_2 - \mathbf{H} \cdot \mathbf{e}_1) \end{bmatrix} \begin{bmatrix} \mathbf{v}_{\text{ext}} \\ v_{\text{r}} \end{bmatrix} \tag{7}$$

We now apply (7) to the model (4). Because **H** is represented by a pole-residue model with a common pole set for all elements, it follows that (7) can be applied to the residue matrices as follows,

$$\mathbf{R}_0^H \rightarrow \begin{bmatrix} \mathbf{R}_0^H & (\mathbf{e}_2 - \mathbf{R}_0^H \cdot \mathbf{e}_1) \end{bmatrix} \tag{8a}$$

$$\mathbf{R}_n^H \rightarrow \begin{bmatrix} \mathbf{R}_n^H & -(\mathbf{R}_n^H \cdot \mathbf{e}_1) \end{bmatrix}, n = 1, \ldots N^H \tag{8b}$$

2) Terminal Admittance Model

The procedure is similar for the terminal admittance model. We have the two conditions

$$\mathbf{i}_{\text{ext}} = \mathbf{Y}(\mathbf{v}_{\text{ext}} - \mathbf{e} \cdot v_{\text{r}}) \tag{9a}$$

$$i_{\text{r}} = -\mathbf{e}^T \mathbf{i}_{\text{ext}} \tag{9b}$$

Combining (9a) and (9b) gives

$$\begin{bmatrix} \mathbf{i}_{\text{ext}} \\ i_{\text{r}} \end{bmatrix} = \begin{bmatrix} \mathbf{Y} & -\mathbf{Y} \cdot \mathbf{e} \\ -\mathbf{e}^T \mathbf{Y}^T & \mathbf{e}^T \cdot \mathbf{Y} \cdot \mathbf{e} \end{bmatrix} \cdot \begin{bmatrix} \mathbf{v}_{\text{ext}} \\ v_{\text{r}} \end{bmatrix} \tag{10}$$

Again, the use of a pole-residue model with a common pole set (3) permits (10) to be applied directly to each residue matrix,

$$\mathbf{R}_n^Y \rightarrow \begin{bmatrix} \mathbf{R}_n^Y & -\mathbf{R}_n^Y \cdot \mathbf{e} \\ -\mathbf{e}^T (\mathbf{R}_n^Y)^T & \mathbf{e}^T \cdot \mathbf{R}_n^Y \cdot \mathbf{e} \end{bmatrix}, n = 0,1, \ldots N^Y \tag{11}$$

E. Inclusion of Model in Circuit Solver

The model is included in the circuit solver known as EMTP-RV using the Damping Factor (DF) model interface described in [15]. Each of the two (augmented) pole-residue models are converted into a state-space model,

$$\mathbf{H}(\omega) = \mathbf{R}_0^H + \sum_{n=1}^{N^H} \frac{\mathbf{R}_n^H}{j\omega - a_n^H} = \left[\begin{array}{c|c} \mathbf{A}^H & \mathbf{B}^H \\ \hline \mathbf{C}^H & \mathbf{D}^H \end{array}\right] \tag{12a}$$

$$\mathbf{Y}(\omega) = \mathbf{R}_0^Y + \sum_{n=1}^{N^H} \frac{\mathbf{R}_n^Y}{j\omega - a_n^Y} = \left[\begin{array}{c|c} \mathbf{A}^Y & \mathbf{B}^Y \\ \hline \mathbf{C}^Y & \mathbf{D}^Y \end{array}\right] \tag{12b}$$

The models (12a) and (12b) are combined into a single state space model,

$$\mathbf{F}(\omega) = \left[\begin{array}{cc|c} \mathbf{A}^Y & \mathbf{0} & \mathbf{B}^Y \\ \mathbf{0} & \mathbf{A}^H & \mathbf{B}^H \\ \hline \mathbf{C}^Y & \mathbf{0} & \mathbf{D}^Y \\ \mathbf{0} & \mathbf{C}^H & \mathbf{D}^H \end{array}\right] \tag{13}$$

which defines the input-output relation,

$$\begin{bmatrix} \mathbf{i}_{\text{ext}}(\omega) \\ \mathbf{v}_{\text{int}}(\omega) \end{bmatrix} = \mathbf{F}(\omega) \cdot \mathbf{v}_{\text{ext}}(\omega) \tag{14}$$

F. Time Domain Validation

The ability of the model to properly simulate the HV N-point voltage due to a ground potential rise was validated by a time domain measurement, see Fig. 9. The transformer was placed on an (insulating) polystyrene plate lying on an aluminum plate. The HV terminals and the LV-side n-point were connected to the tank, assuming a situation where the HV-side surge arresters and the LV-side neutral point arrester are conducting with negligible voltage drops. The grounding impedance at the transformer and on the LV side were both represented by 30 Ω resistors. An impulse source was applied between the aluminum sheet and the transformer tank and the associated current was measured using a wide band current transformer (Ion Physics, model CM-100-6L). The resulting voltage on the tank and on the transformer N-point were measured using voltage probes.

Fig. 10 shows the measured current. This current was used as an ideal current source in a time domain simulation where the transformer model is subjected to the same terminal condition as in Fig. 9. Fig. 11 compares the simulated voltage response on tank and HV-side N-point with the measurement. It is observed that the model reproduces the measured voltages with excellent accuracy.

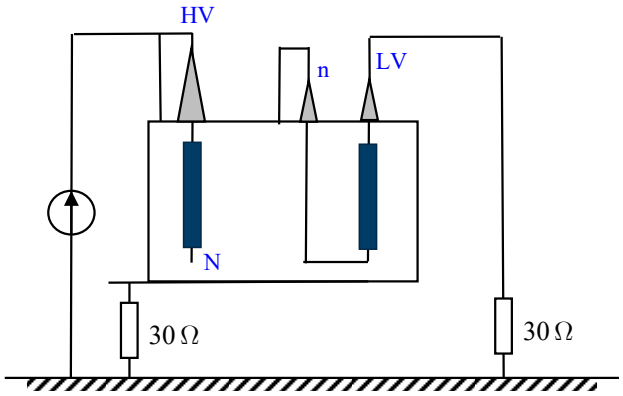

Fig. 9. Measurement setup with current injection from ground to transformer tank. HV terminals and LV winding n-point connected to tank.

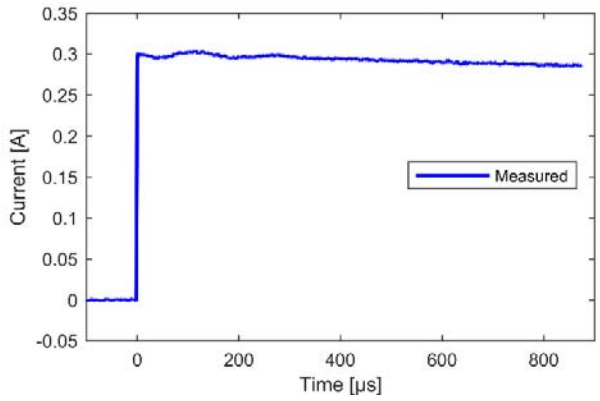

Fig. 10. Current excitation.

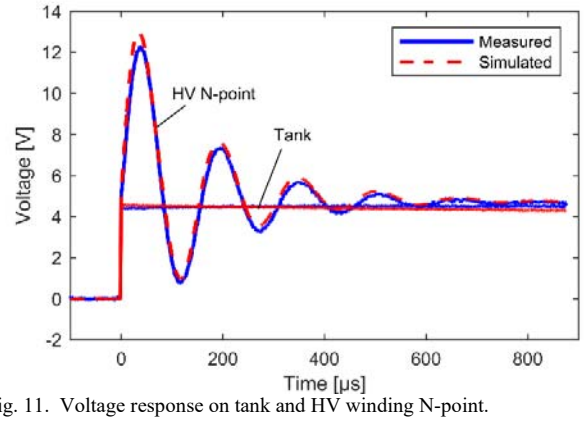

Fig. 11. Voltage response on tank and HV winding N-point.

VI. N-Point Voltage Considerations

The model of the voltage transfer block **H** gives by itself an impression about the possibility of a very high voltage in the HV neutral point relative to the transformer tank. As an example, a simulation is made where a 1-Volt zero sequence voltage is applied between the LV terminals and ground, with the LV n-point and the HV terminals grounded, see Fig. 12. The applied voltage on the LV terminals corresponds to the LV winding voltage drops in Fig. 1, which gives rise to a transformed voltage to the HV windings. The simulation result in Fig. 13 shows that a peak voltage of nearly 60 Volt results in the N-point after 33 µs. The voltage in the HV-winding midpoints is about 50% of this value, which is to be expected since a transformed voltage is linear along the winding. The following additional observations can be made.

1. The oscillation frequency is fairly low (14 kHz). This implies that a voltage excitation on the LV side must be of substantial duration for the voltage rise in the N-point to reach its potential maximum value; about 35 µs with the given oscillation period of T=71 µs.
2. The slow component of the HV N-point voltage (about 38 Volt) is lower than the 48-Volt that corresponds to a coupling by the winding ratio (48:1). This reduced coupling can be an effect of increased stray fluxes compared to normal operation since the flux path of a three-legged transformer includes air gaps and the tank in series with the core.

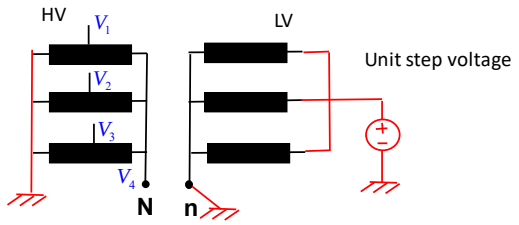

Fig. 12. Zero sequence unit step voltage excitation on the LV side.

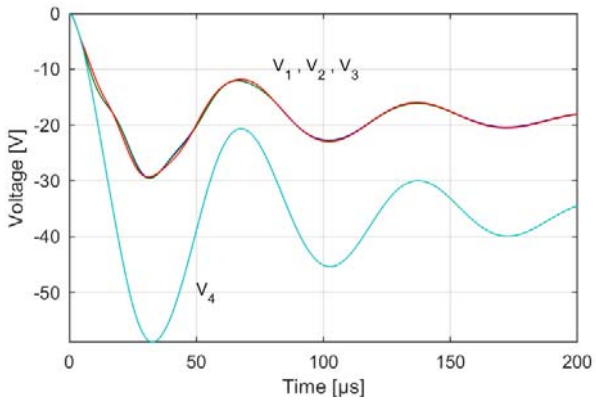

Fig. 13. Voltage response in HV N-point (V_4) and HV windings midpoint.

VII. Transformer Protection

We return to Fig. 1 in Section II which shows the overvoltage protection of a distribution transformer as frequently found in Norwegian rural areas. On the HV-side, surge arresters are placed between each phase and the transformer tank. The LV-side neutral point (n) is connected to the tank through a mandatory neutral point arrester, which is a ZNO-element in series with a gap and fuse. If the fuse blows, spring-loaded contact arms will connect the n-point permanently to the tank. The intention is to avoid that high voltage is transferred to the 230 V side in the case of a transformer internal failure. In this work we assume that the fuse has not blown. The n-point series gap is considered as a short-circuit as it has a quite low flashover voltage (1000 Volts, typically) relatively to the ground potential rise. The figure also includes optional LV-side phase-neutral surge arresters (grey-color). These arresters are frequently omitted. The HV-side N-point is usually an internal connection point only. When brought out as a terminal, it will

normally be unprotected.

Tables II and III define the surge arrester protective characteristics that will be used in the ensuing calculations, taken from the manufacturer's catalogue for an 8/20 μs current wave. The chosen HV-side arrester characteristic corresponds to a rated value of 16.3 kV and continuous operating voltage U_c=13 kV (ABB Polim-K arrester). The reason for such high value of U_c is that the system can be operated with a standing single-phase ground fault for several hours. The I-V curve for the HV-side arresters (Table II) is assumed to apply also for the LV-side surge arresters, when scaled with the ratio between the protective levels (1.2 kV/40 kV=0.03). The surge arresters are represented by piecewise non-linear resistors in EMTP-RV.

TABLE II
SURGE ARRESTER PROTECTIVE LEVELS @ 5 KA.

Voltage level		U_p [kV]
12 kV	line-ground arresters	40 kV
230 V	line-ground arresters, n-point arrester	1.2 kV

TABLE III
HV SIDE SURGE ARRESTER I-V CHARACTERISTIC.

V [Volt]	Current [A]	V [Volt]	Current [A]
16500	0.1	40300	5000
33950	500	42750	10000
35300	1000	47900	20000
36950	2000	55000	40000

VIII. GROUND POTENTIAL RISE AND N-POINT OVERVOLTAGES

A. *Transfer of LV Winding Voltages to HV Windings*

As an example, consider the situation that the lightning current in Fig. 1 is injected directly into the transformer HV-side terminals so that the entire lightning current is forced to flow through the three HV-side surge arresters. The current is assumed to have a peak value of 20 kA, 5 μs linear front and a linear tail with 100 μs to half-value. The grounding impedances are $Z_{g,\text{tank}} = 25\Omega$, $Z_{g,\text{LV}} = 25\Omega$. The system response is simulated using EMTP-RV with the transformer model included via the damping factor model interface [15].

Fig. 14 shows the simulated current flow through the HV-side arresters, the tank grounding impedance, and from tank to the LV-side n-point (via the n-point arrester). The result is shown without and with usage of LV-side arresters between LV terminals and n-point. Clearly, the use of LV-side arresters reduces the current through the n-point arrester and thus also through the LV windings.

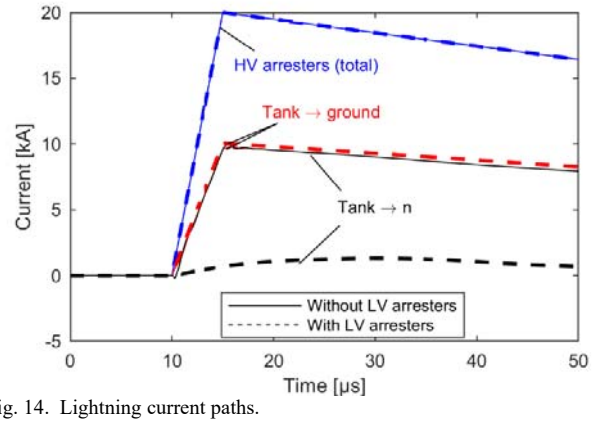

Fig. 14. Lightning current paths.

Fig. 15 shows the resulting LV-side voltages with respect to the tank voltage. With usage of LV-side arresters, the long-duration part of the voltage along the LV windings is reduced from about 10 kV to the arrester protective level (1.2 kV). The 20 kV initial voltage can be explained by capacitive coupling from the HV windings to the LV windings. It is likely that the LV-side bushings can withstand such high voltage since they are normally 1 kV equipment that have been tested with 20 kV 1.2/50 μs voltage (CENELEC 2002-07-12).

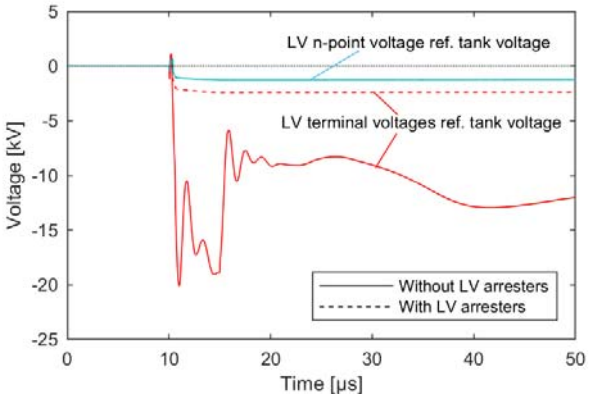

Fig. 15. Transformer LV-side voltages ref. tank voltage.

Fig. 16 shows the simulated tank voltage and transformer HV-side voltages, with respect to remote ground. Without the LV-side arresters, the N-point voltage reaches 541 kV with respect to the tank voltage but is reduced to 109 kV when LV-side arresters are used. The voltage reduction is caused by the reduced voltage along the LV windings observed in Fig. 15. Still, the voltage (109 kV) is above the transformer impulse test voltage (75 kV).

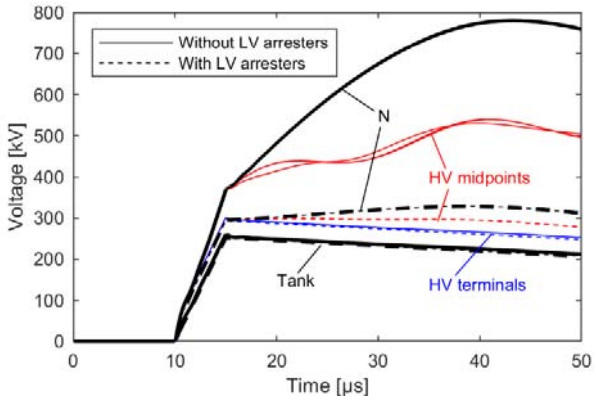

Fig. 16. Transformer HV side voltages vs. remote ground.

B. Significance of Transformer Zero-Sequence Impedance

The voltage that results along the LV-windings is dependent on the LV-winding zero sequence impedance, in addition to the lightning current flowing through these windings. Fig. 17 shows the zero-sequence impedance between LV terminals and n-point as calculated by the model, with HV-terminals grounded to the (same) n-point. It is observed that the impedance is quite low, varying between 1 Ω and 15 Ω in the 1 kHz -100 kHz frequency range. The low impedance implies that it takes a high current (order of kA) to produce a voltage of the order of kV along the LV windings. The reason for the very low impedance value is the presence of air gaps in the zero-sequence flux path, which results with a three-legged core design. The model's accuracy is in the figure validated by a direct impedance measurement.

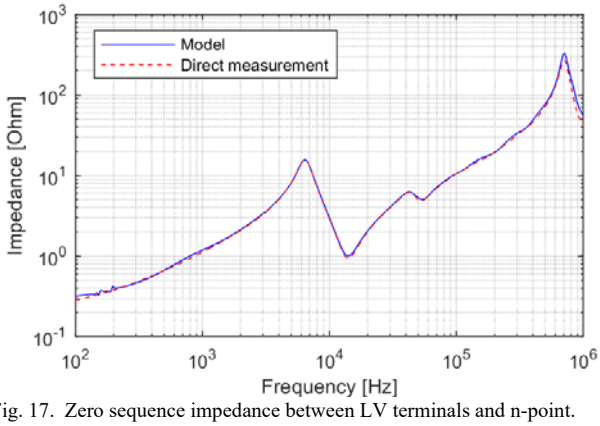

Fig. 17. Zero sequence impedance between LV terminals and n-point.

C. Significance of Grounding Impedances

The N-point voltage vs. tank increases with increasing current through the LV windings. Without LV-side arresters, the N-point voltage will therefore increase with increasing lightning current and tank grounding impedance, and with decreasing LV side grounding impedance at the point of current discharge to earth. This consideration is verified by Table IV which lists the maximum N-point voltage with respect to the tank, for different parameter combinations of lightning current and grounding impedances. (The lightning current shape is as before: 5 μs linear front and linear tail with 100 μs to half-value). Table V shows the corresponding result when LV-side arresters are used. The voltages are now limited very much since the current through the LV-windings are reduced.

TABLE IV
WITHOUT USAGE OF LV-SIDE SURGE ARRESTERS.
MAXIMUM VOLTAGE BETWEEN N-POINT AND TANK.

I_m=10 kA			I_m=20 kA		
$Z_{g,transf}$ [Ω]	$Z_{g,LV}$ [Ω]	V_{max} [kV]	$Z_{g,transf}$ [Ω]	$Z_{g,LV}$ [Ω]	V_{max} [kV]
25	25	288	25	25	541
25	50	207	25	50	378
50	25	**375**	50	25	**714**
50	50	292	50	50	548

TABLE V
WITH USAGE OF LV-SIDE SURGE ARRESTERS.
MAXIMUM VOLTAGE BETWEEN N-POINT AND TANK.

I_m=10 kA			I_m=20 kA		
$Z_{g,transf}$ [Ω]	$Z_{g,LV}$ [Ω]	V_{max} [kV]	$Z_{g,transf}$ [Ω]	$Z_{g,LV}$ [Ω]	V_{max} [kV]
25	25	100	25	25	107
25	50	98	25	50	105
50	25	**102**	50	25	**109**
50	50	100	50	50	107

Fig. 18 shows the N-point voltage vs. tank as function of the transformer grounding impedance $Z_{g,transf}$ with two alternative lightning currents. The LV-side grounding impedance is $Z_{g,LV} = 25\Omega$. Without LV-side arresters, the transformer N-point voltage vs. tank is low only if both the grounding impulse impedance and the injected lightning current are small. (The smallest grounding impedances in Fig. 18 are difficult to reach in practice). With usage of the LV-side arresters, the voltage is limited to about 100 kV, even with poor grounding and a high lightning current.

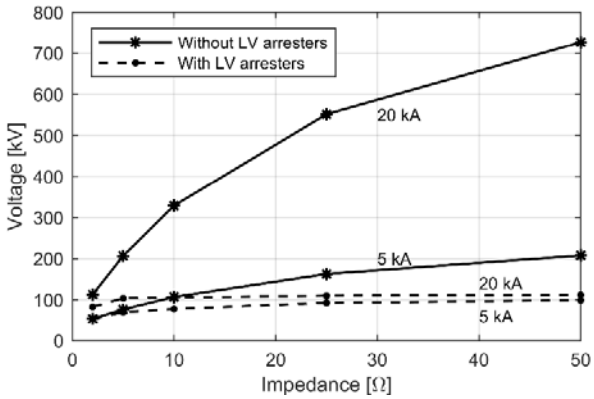

Fig. 18. N-point voltage ref. transformer tank as function of transformer grounding impulse impedance, $Z_{g,transf}$. Parameter: Lightning flowing through HV-side surge arresters.

IX. ALTERNATIVE PROTECTION SCHEMES

A. System

Having understood the fundamental mechanism behind the N-point voltage buildup, some traditional protection schemes are compared where the transformer is placed in a system, see Fig. 19. On the HV-side, the transformer is connected to an OHL that is subjected to a lightning stroke 200 m away from the transformer. The transformer is fitted with HV-side surge

arresters and the (mandatory) LV-side n-point arrester. On the LV-side, the customer installations are represented by a single surge arrester in series with a (separate) 25 Ω grounding impedance that is placed in vicinity of the transformer. In the following will be shown the voltage between the HV-side N-point and the tank, when additional protection is used: LV-side surge arresters, spark gap in the first tower, ground wire on the HV side.

The OHL is modeled as a frequency-dependent transmission line model in EMTP-RV [16] ("fd-line"). The lightning current is assumed to be the same as in the previous examples: 20 kA peak value, linear front and tail with 5 µs front time and 100 µs time to half-value.

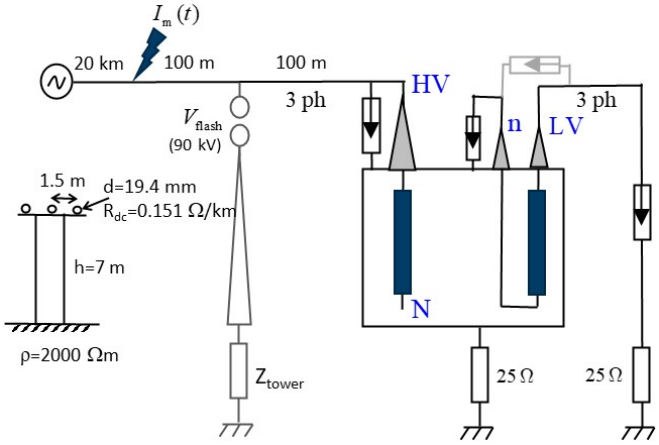

Fig. 19. Lightning stroke HV-side overhead line.

B. LV-side Surge Arresters

As a reference calculation, LV-side arresters are connected between the LV-side terminals and n-point.

C. Spark Gap in Nearest HV-Side Tower

In the past, spark gaps were extensively used on the HV overhead lines to reduce the peak value of the incoming overvoltage that meets the transformer. We assume that spark gaps are installed only in the nearest tower, 100 m away from the transformer as shown in Fig. 19. LV-side arresters are not installed. The spark gaps are assumed to have a 90 kV fixed flashover voltage. The ground sides are brought down to the earth electrode via a copper lead represented by a series inductance of 15 µH. The remaining line masts have wood poles without tower top grounding. The flashover voltage to ground is therefore very high, with an assumed value of 2 MV in this study. It is further assumed that the lightning strikes causes a flashover between all three phases at the stroke location.

Fig. 20 shows with blue traces the simulated N-point voltage with respect to the tank potential, with the tower footing grounding impedance Z_{tower} as parameter. As the tower footing impedance is reduced, a larger part of the lightning current flows to ground at the spark gap, thereby reducing the current flowing to the transformer ground and hence the associated ground potential rise and resulting current through the LV-side arresters. The N-point voltage is seen to be reduced in about half when the tower impedance is equal to the transformer grounding impedance (25 Ω). The plot also includes the result without any spark gap, and with the use of LV arresters instead of the spark gaps. It is observed that the tower footing impedance must be as small as 5 Ω in order to limit the N-point overvoltage to a level close to that obtained by LV arresters alone. Such low impedance can be difficult and costly to achieve.

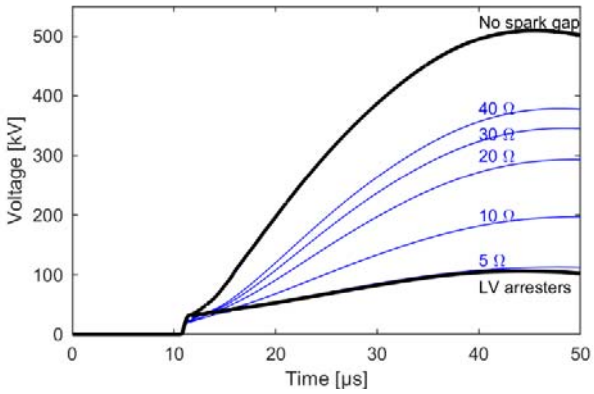

Fig. 20. N-point voltage ref. transformer tank. Parameter: spark gap tower footing grounding impedance, Z_{tower}.

D. Continuous HV-Side Ground Wire

Some HV-side overhead lines are fitted with a ground wire. The simulation circuit in Fig. 19 was modified accordingly by fitting the OHL with a ground wire located 2 m below the phase conductors. The ground wire is grounded in each tower and it is terminated on the transformer tank. All crossarms are now assumed conductive and connected to the ground wire. Wire data: d=8.7 mm, R_{dc}=0.721 Ω/km. The line insulators are assumed to have a lightning impulse flashover voltage of 120 kV, and there are no spark gaps installed. Eight spans are included in the simulation with 100 m span length. The result is shown in Fig. 21, with tower footing impedance as parameter. Comparison with Fig. 20 (spark gap only) reveals a substantial improvement in overvoltage reduction. With 40 Ω grounding impedances, the N-point voltage vs. tank is now limited to 165 kV, compared to 380 kV with spark gaps in nearest tower alone. If one in addition introduces LV arresters (dashed traces), a further voltage reduction to about 75 kV is achieved. The improvement with the use of ground wire is caused by insulator flashovers along the line as well as repeated wave reflections between the tower footing groundings. That way, the current injection into the transformer tank grounding electrode is reduced.

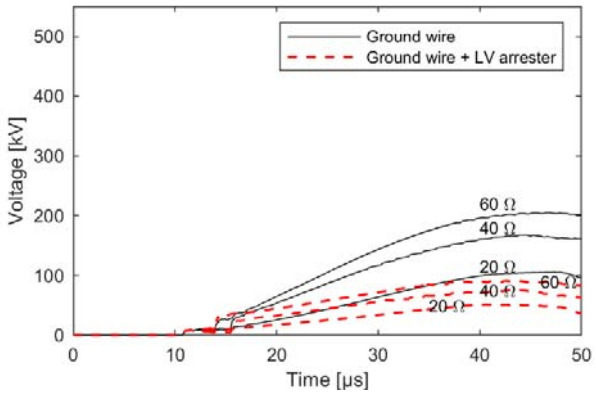

Fig. 21. N-point voltage ref. transformer tank. Continuous ground wire. Parameter: tower footing grounding impedance, Z_{tower}.

X. Discussion

A. Failure statistics

The above considerations regarding overvoltage protection are in line with the experience of Norwegian utilities since 1985. It has been reported in several forums that the introduction of LV-side surge arresters is a very effective way of reducing the transformer failure rate. The failure area is usually found in the HV-windings.

B. Lightning Overvoltages Originating From The LV Side

A direct lightning stroke to an LV-side OHL may also give high N-point overvoltages since a high current may then flow through the LV windings to the tank grounding. Also in this case, the use of LV-side surge arresters is expected to be an effective counter measure as the voltage along the LV-windings becomes limited.

C. Modeling

In this work we used simple models for the network around the transformer since we wished to explain the N-point overvoltage phenomenon in a simple and understandable way. More realistic simulation studies of lightning overvoltages on transformers requires a sufficiently detailed and accurate representation of the relevant network components (e.g. lead inductances and insulator flashover characteristics) as well as the lightning current with shape parameters and their statistical variations. For more information about the modeling of components and lightning parameters we refer to [2], [17], [18] and references therein.

D. Inclusion of Model in Simulation Programs

The time domain calculations were performed using the electromagnetic transients program known as EMTP-RV, via the (user-defined) DF model interface described in Section V.E. The inclusion in simulation programs can also be done in other ways. For instance, the terminal admittance part can be included as a state-space model or via an equivalent circuit. The transferred voltage to internal points (N-point) can afterwards be calculated via (recursive) convolution in a post processing step. Reference [19] shows details for such implementation, including link to downloadable Matlab code.

XI. Conclusion

A lightning current being discharged to earth via the transformer HV-side surge arresters will cause a potential rise of the transformer tank with respect to ground. In the case of a wye-wye connected transformer where the HV-side neutral point is unprotected, the tank potential rise can drive a current through the LV windings whose associated voltage drops become transformed to the HV windings. The transformed voltage initiates an oscillating voltage in the HV-side N-point with respect to the tank that can reach several times the transformer impulse test voltage.

LV-side surge arresters firmly limit the overvoltage along the LV windings according to the arrester current-voltage characteristic, thereby being an effective way of limiting the transformed voltage to the HV windings. Still, the voltage in the N-point may exceed the transformer test voltage. The additional use of spark gaps on the overhead line or a ground wire on the HV-side can further reduce the overvoltage by limiting the tank ground potential rise. The use of a low-impedance impulse grounding at the transformer has a similar effect.

Acknowledgement

The insight about the N-point voltage phenomenon was brought to our attention by Dr. Thor Henriksen, Jostein Huse, Lars Rolfseng, Kjell Alstad and Sigbjørn Asbjørnslett, past employees at SINTEF Energy Research.

Appendix

The measurements are performed using small-signal frequency sweep measurements based on a vector network analyzer (VNA) with gain-phase setup, Agilent E5061B-3L5.

The measurements of the admittance matrix **Y** make use of a connection box with inclusion of a wide-band current sensor (Ion Physics, model CM-100-6L). The setup measures the elements of the admittance matrix one-by-one by the approach described in [19]. The connection to the transformer is made by coaxial cables as shown in Fig. 22. The 0.1 Ω series resistors on the LV side are included in admittance measurements to alleviate measurement inaccuracies at lower frequencies. It is remarked that to properly reproduce the capacitive charging currents associated with floating windings, a 2×2 common-mode admittance measurement was made with respect to the two windings and merged with the original 7×7 **Y**. The procedure is based on the one in [20].

The measurement of the voltage transfer matrix **H** makes use of two identical voltage probes, similarly to the measurements in [21]. In these measurements, the 0.1 Ω series resistances and cables are not used.

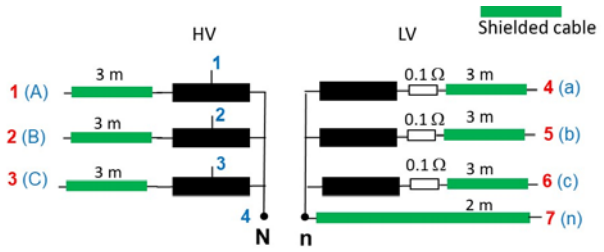

Fig. 22. Admittance measurements.

REFERENCES

[1] M. A. Uman, *The lightning discharge*, Dover, 2001.
[2] J. A. Martinez-Velasco, *Transient analysis of power systems: Solution techniques, tools and applications*, Wiley-IEEE, 2014.
[3] V. Cooray, *Lightning protection*, IET, 2009.
[4] T. Noda, H. Nakamoto and S. Yokoyama, "Accurate modeling of core-type distribution transformers for electromagnetic transient studies," *IEEE Trans. Power Delivery*, vol. 17, no. 4, pp. 969-976, Oct. 2002.
[5] M.J. Manyahi and R. Thottappillil, "Transfer of lightning transients through distribution transformers," *Proc. Int. Conf. Lightning Protection*, September 2-6, 2002, Cracow, pp. 435-440.
[6] N. A. Sabiha and M. Lehtonen, "Lightning-Induced Overvoltages Transmitted Over Distribution Transformer With MV Spark-Gap Operation—Part I: High-Frequency Transformer Model," *IEEE Trans. Power Delivery*, vol. 25, no. 4, pp. 2472-2480, Oct. 2010.
[7] A. K. Agrawal, H. J. Price, and S. H. Gurbaxani, "Transient response of multiconductor transmission lines excited by a nonuniform electromagnetic field," *IEEE Trans. Electromagn. Compat.*, vol. 22, no. 2, pp. 119–129, May 1980.
[8] V. Cooray, "Horizontal fields generated by return strokes," Radio Sci., vol. 27, no. 4, pp. 529–537, July 1992.
[9] A. Borghetti, A. Morched, F. Napolitano, C. A. Nucci and M. Paolone, "Lightning-Induced Overvoltages Transferred Through Distribution Power Transformers," *IEEE Trans. Power Delivery*, vol. 24, no. 1, pp. 360-372, Jan. 2009.
[10] Technical Brochure 577A, "Electrical transient interaction between transformers and the power system. Part 1 – Expertise", CIGRE JWG A2/C4.39, April 2014.
[11] B. Gustavsen, "Rational modeling of multi-port systems via a symmetry and passivity preserving mode-revealing transformation", *IEEE Trans. Power Delivery*, vol. 29, no. 1, pp.199-205, February 2014.
[12] B. Gustavsen and A. Semlyen, "Rational approximation of frequency domain responses by vector fitting", *IEEE Trans. Power Delivery*, vol. 14, no. 3, pp. 1052-1061, July 1999.
[13] D. Deschrijver, M. Mrozowski, T. Dhaene, and D. De Zutter, "Macromodeling of multiport systems using a fast implementation of the vector fitting method", *IEEE Microwave and Wireless Components Letters*, vol. 18, no. 6, pp. 383-385, June 2008.
[14] B. Gustavsen, "Fast passivity enforcement for pole-residue models by perturbation of residue matrix eigenvalues", *IEEE Trans. Power Delivery*, vol. 23, no. 4, pp. 2278-2285, October 2008.
[15] B. Gustavsen, C. Martin, A. Portillo, "Time domain implementation of damping factor white-box transformer model for inclusion in EMT simulation programs", *IEEE Trans. Power Delivery*, accepted, Digital Object Identifier: 10.1109/TPWRD.2019.2902447.
[16] J.R. Marti, Accurate modelling of frequency-dependent transmission lines in electromagnetic transient simulations", *IEEE Trans. PAS*, vol. 101, no. 1, pp. 147-157, Jan. 1982.
[17] CIGRE TB 63, "Guide to procedures for estimating the lightning performance of transmission lines", CIGRE WG 01 of SC 33, October 1991.
[18] IEEE Working Group 15.08.09, "Modeling and analysis of system transients using digital programs," IEEE PESTP-133-0, 1998.
[19] B. Gustavsen and H.M.J. De Silva, "Inclusion of rational models in an electromagnetic transients program – Y-parameters, Z-parameters, S-parameters, transfer functions", *IEEE Trans. Power Delivery*, vol. 28, no. 2, pp. 1164-1174, April 2013.
[20] B. Gustavsen, "Wide band modeling of power transformers", *IEEE Trans. Power Delivery*, vol. 19, no. 1, pp. 414-422, Jan. 2004.
[21] B. Gustavsen, A. Portillo, R. Ronchi, A. Mjelve, "High-frequency resonant overvoltages in transformer regulating winding caused by ground fault initiation on feeding cable", *IEEE Trans. Power Delivery*, vol. 33, no. 2, pp. 699-708, April 2018.

BIOGRAPHY

Bjørn Gustavsen (M'94–SM'2003–F'2014) was born in Norway in 1965. He received the M.Sc. degree and the Dr. Ing. degree in Electrical Engineering from the Norwegian Institute of Technology in Trondheim, Norway, in 1989 and 1993, respectively. Since 1994 he has been working at SINTEF Energy Research, currently as Chief Research Scientist. He is also an adjunct Professor at NTNU, since 2020. His interests include simulation of electromagnetic transients and modeling of frequency dependent effects.

Kårstein Longva Kårstein Longva was born in Norway in 1955. He received the M.Sc.degree in Electrical Power Engineering from Norwegian Institute of Technology in Trondheim, Norway in 1979. He has since 1983 been engaged at Møre Trafo as Design Manager and Product Manager. His employment includes development of Engineering Systems and Calculation Programs for Distribution Transformers.